CHAPTER V

RESULTS AND DISCUSSION

5.1 Degree of Clay Dispersion in Nylon 6/Clay Nanocomposite Films

A degree of layered silicate dispersion in polymer matrix strongly affects the mechanical and barrier properties of polymer/clay nanocomposites [2-6, 8-14]. Especially, polymer/clay nanocomposites, which clay is exfoliated throughout the polymer matrix, are desirable for improving various properties due to high aspect ratio of clay and large interfacial area between polymer and layered silicates. X-ray diffraction (XRD) is the characterization technique, used to determine an interlayer spacing of layered silicates or identify intercalated structure. Interlayer spacing and diffraction peak of pristine clay, organoclays and nanocomposite films were summarized in table C.1 (appendix C).

XRD patterns of pristine clay and two organoclays, which were M_3T and $M_2(HT)_2$ organoclay, were illustrated in figure 5.1. It can be seen that the peak showing an interlayer spacing of pristine clay was at $2\theta = 7.15^\circ$ corresponding to an interlayer spacing of 1.23 nm. M_3T organoclay exhibited a broad and low intensity peak at $2\theta = 1.67^\circ$, 3.31° and 4.65° corresponding to an interlayer spacing of 5.27, 2.67 and 1.90 nm respectively. However, $M_2(HT)_2$ organoclay exhibited an intense peak at $2\theta = 2.45^\circ$ and small peak at $2\theta = 4.88^\circ$ corresponding to an interlayer spacing of 3.59 and 1.81 nm respectively. The difference in an interlayer spacing could be due to the difference in actual surfactant concentration that penetrated between layered silicates. Moreover, the three different broadening diffraction peaks of M_3T organoclay that showed in figure 5.1 may be resulted from the difference of orientation of amine surfactant between layered silicates. This result was different from Fornes et al. [4] and Osman et al. [5] that organoclay treated with the higher

number of long alkyl groups of amine compound leaded to the widening of the interlayer spacing.

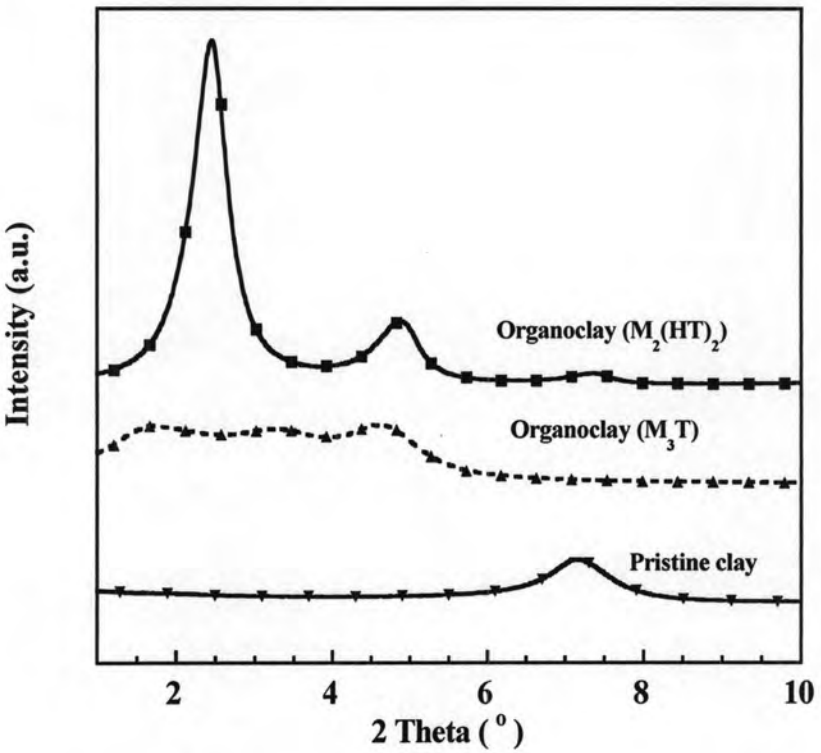

Figure 5.1: XRD patterns of clay and two organoclays, which were M_3T and $M_2(HT)_2$ organoclay.

After obtaining two organoclays, M_3T organoclay was melted mixing with nylon 6 and extruded through a twin screw extruder attached to blown film die at 1, 3, 5 and 7 wt% of organoclay loading. From figure 5.2 and 5.5, at 1 wt% of organoclay loading, the XRD pattern of M_3T nanocomposite film was nearly flat, only small shoulder was observed at $2\theta = 1.96°$. This could be due to a nearly exfoliated state of clay in nylon 6. However, M_3T nanocomposite films predominantly consisted of an intercalated structure when adding more than 1 wt% of organoclay. XRD peak of M_3T nanocomposite films with 3, 5 and 7 wt% of organoclay loading was observed at $2\theta =$ 2.02°, 2.46°and 2.60° corresponding to an interlayer spacing of 4.38, 3.58 and 3.40 nm respectively. Therefore, the diffraction peak shifted to higher angle when organoclay loading was increased from 1 to 7 wt%. In other words, the distance between layered

silicates decreased as organoclay loading increased. This could be due to the degradation of ammonium ion within layered silicates which is consistent with Shah et al. [3] and Fornes et al. [4]. The decrease in interlayer spacing of layered silicates in M_3T nanocomposite films could be resulted from the rearrangement of surfactant between layered silicates while mixing nylon 6 with M_3T organoclay. Moreover, the decrease in interlayer spacing of layered silicates in M_3T nanocomposite films could be due to the change of free energy after mixing nylon 6 with M_3T organoclay. The entropy of layered silicates which was small positive, decreased to be negative after M_3T organoclay was added to form M_3T nanocomposite films. This could be caused by the configuration of nylon 6 chains in M_3T nanocomposite films limited by layered silicates. These results were confirmed by TEM image as shown in figure 5.3. It can be seen that layered silicates in M_3T nanocomposite films at 3 wt% of organoclay loading still contained a stacks of layered silcates that intercalated with nylon 6 matrix. However, there was a small fraction of two or three silicate layers that dispersed into M_3T nanocomposite films. Furthermore, the diffraction intensity of M_3T nanocomposite films was gradually increased with increasing organoclay loading. The increase in diffraction intensity of XRD peak leaded to high order of layered silicates that dispersed into nylon 6 matrix. From figure 5.2, it can be seen that the orientation of layered silicates of M_3T nanocomposite films at 7 wt% of organoclay loading was more orderly than that of M_3T nanocomposite films at 3 wt% of organoclay loading. Therefore, the broadening of the diffraction peak at 3, 5 and 7 wt% of organoclay loading could identify that the orientation of layered silicates in nylon 6 films had a good disorder. Moreover, the area under diffraction intensity of M_3T nanocomposite films increased with increasing organoclay loading. This indicated that the amount of layered silicates which was a component of organoclay, increased when organoclay was added into nylon 6 matrix. Both good distribution and increase in layered silicate content strongly affected the properties of M_3T nanocomposite films such as mechanical and barrier properties.

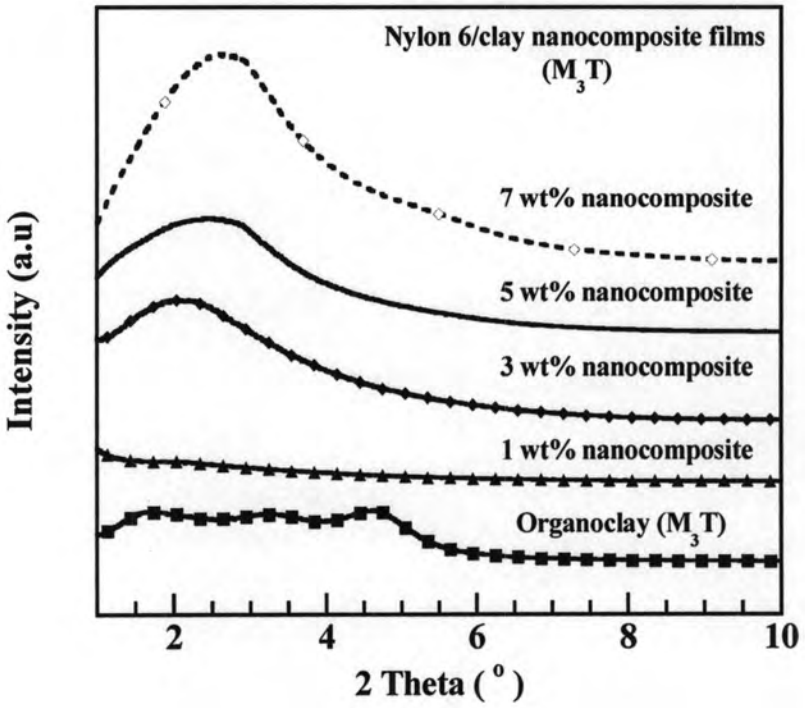

Figure 5.2: XRD patterns of M_3T organoclay and M_3T nanocomposite films at different organoclay loading.

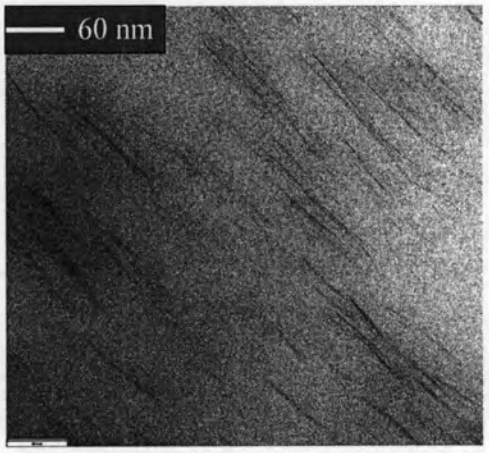

Figure 5.3: TEM micrograph of M_3T nanocomposite films at 3 wt% of organoclay loading.

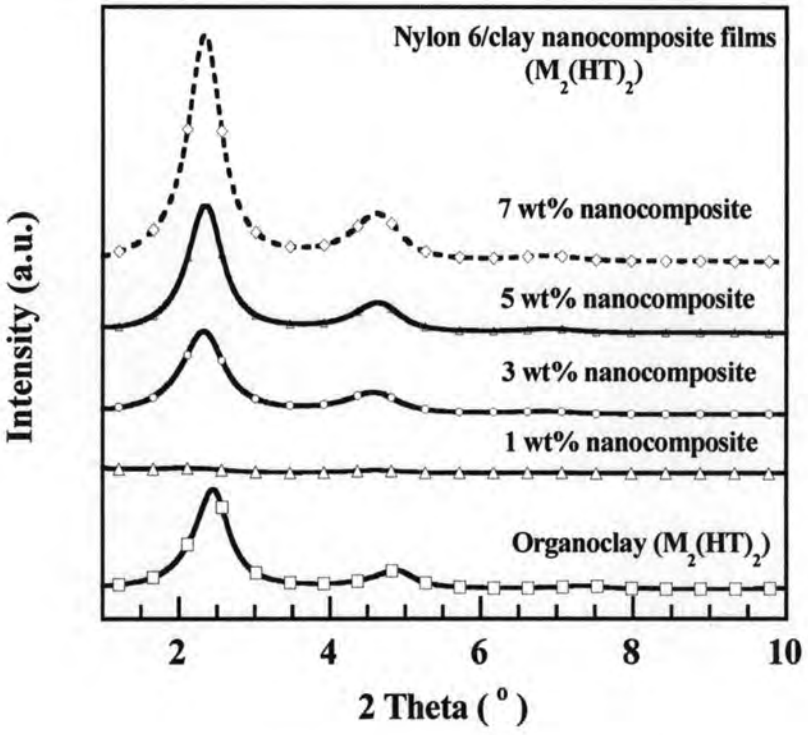

Figure 5.4: XRD patterns of $M_2(HT)_2$ organoclay and $M_2(HT)_2$ nanocomposite films at different organoclay loading.

XRD pattern of 1 wt% of $M_2(HT)_2$ nanocomposite films exhibited two peaks at around $2\theta = 2.00^\circ$ and 4.59° corresponding to an interlayer spacing of 4.40 and 1.92 nm respectively as shown in figure 5.4 and 5.5. This interlayer spacing was higher than interlayer spacing of $M_2(HT)_2$ organoclay. In other words, the interlayer spacing between layered silicates increased after nylon 6 was melted mixing with $M_2(HT)_2$ organoclay. However, layered silicates still formed as an intercalated structure in $M_2(HT)_2$ nanocomposite films. When organoclay was further added into nylon 6 matrix at 3 wt%, the diffraction peak shifted to the higher angle value at $2\theta = 2.33^\circ$ and 4.57° corresponding to an interlayer spacing of 3.79 and 1.93 nm respectively. And the diffraction peak still appeared at the same angle value (2θ) after adding organoclay over 3 wt% as shown in figure 5.4. However, it can be seen that the diffraction intensity increased with increasing organoclay loading. This trend was the same as M_3T nanocomposite films as discussed above.

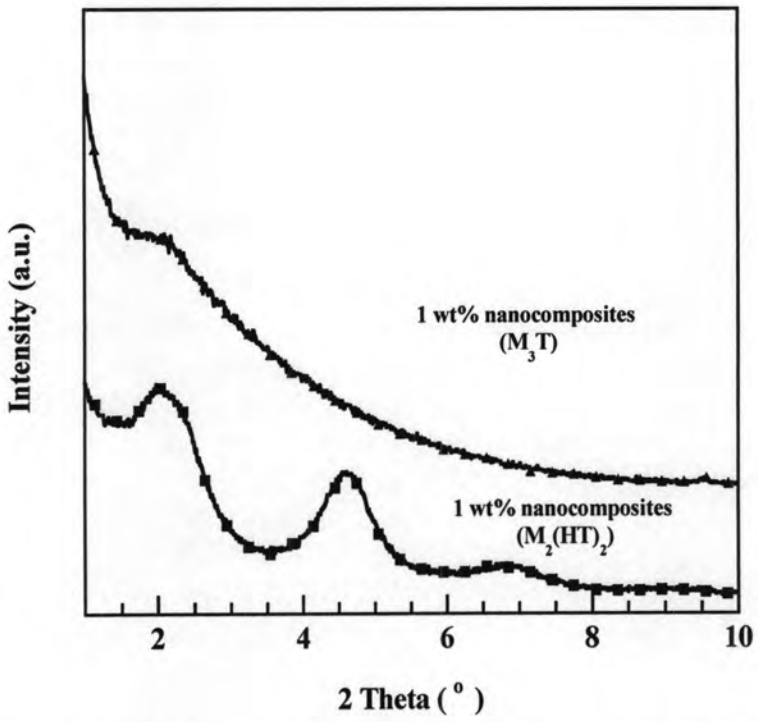

Figure 5.5: XRD patterns indicating an interlayer spacing of clay in M_3T and $M_2(HT)_2$ nanocomposite films at 1 wt% of organoclay loading.

From XRD results, M_3T nanocomposite films showed better dispersion of layered silicates than $M_2(HT)_2$ nanocomposite films for all organoclay loading. Especially, at 1 wt% of nanocomposite films as shown in figure 5.5, the diffraction peak of M_3T nanocomposite films was nearly flat while $M_2(HT)_2$ nanocomposite films exhibited two weak peaks. Moreover, at 3, 5 and 7 wt% of organoclay loading, the peak of M_3T nanocomposite films was broader than $M_2(HT)_2$ nanocomposite films as shown in figure 5.2 and 5.4. This indicated that M_3T nanocomposite films exhibited better dispersion than $M_2(HT)_2$ nanocomposite films. These observations can be strongly affected mechanical, barrier and other properties of nanocomposite films.

5.2 Thermal Properties of Nylon 6/Clay Nanocomposite Films

Thermal properties of neat nylon 6 and nanocomposite films at different organoclay loading were determined by means of differential scanning calorimetry, DSC. The melting (T_m) and crystallization temperature (T_c) of nanocomposite films at different organoclay loading were summarized in table E.1 (appendix E). DSC heating curves at the rate of 10°C/min of neat nylon 6 and M_3T nanocomposite films were shown in figure 5.6.

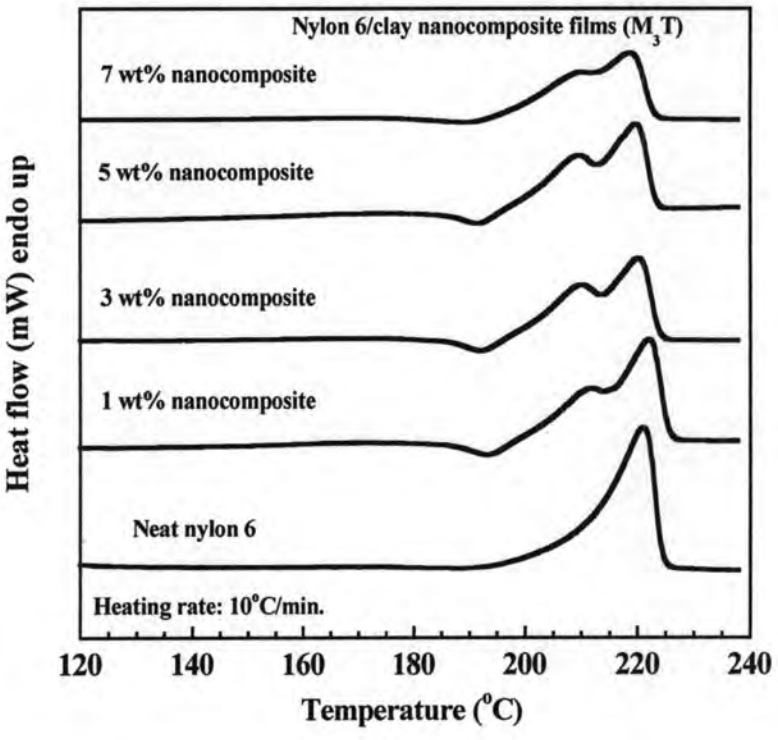

Figure 5.6: DSC heating profiles of nylon 6 and M_3T nanocomposite films at different organoclay loading.

Neat nylon 6 film showed only one melting peak at 221.2°C, corresponding to the α-crystalline phase of nylon 6, which was different from XRD results. Nylon 6 was heated from room temperature to 240.0°C; therefore, polymer chains can be rearranged and formed more stable α-crystalline phase during heating. After mixing nylon 6 with M_3T organoclay, the nanocomposite films exhibited two melting peaks

at 209.6 and 220.3°C, which were γ and α-crystalline phase of nylon 6 respectively for all organoclay loading. However, α-crystalline phase of nylon 6 was still dominant for all nanocomposites. Furthermore, the area under α-crystalline peak decreased with increasing organoclay loading and γ-crystalline phase of nylon 6 became a sharper melting peak when organoclay loading was added to 5wt%. After that γ-crystalline peak of nylon 6 is slightly decreased when organoclay loading was further added over 5 wt%. This result indicated that the addition of layered silicates into nylon 6 matrix enhanced the formation of γ-crystalline phase of nylon 6, which is consistent with Fornes et al. [7], Jiang et al. [8] and Liu et al. [10].

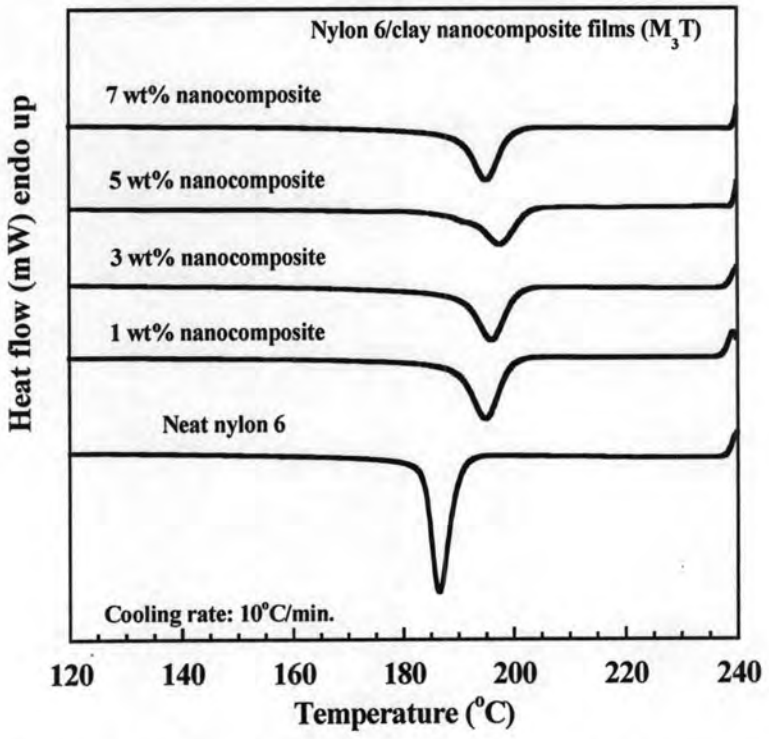

Figure 5.7: DSC cooling profiles of nylon 6 and M_3T nanocomposite films at different organoclay loading.

After heating to 240.0°C, M_3T nanocomposite films were then cooled at 10°C/min in which the cooling profiles were shown in figure 5.7. An exothermic crystallization peak of neat nylon 6 films exhibited one crystallization temperature at 186.2°C. Interestingly, when M_3T organoclay was added into nylon 6 matrix, crystallization temperature was shifted to higher temperature than neat nylon 6 about

8.7°C. However, crystallization temperature of M_3T nanocomposite films shifted to the higher temperature when organoclay loading approached 5 wt%. After that the crystallization peak shifted to the lower temperature with adding organoclay loading further.

These similar trends of heating profiles were also observed for $M_2(HT)_2$ nanocomposite films as shown in figure 5.8. The nanocomposite films exhibited two melting peaks at 210.0 and 220.0°C, which were γ and α-crystalline phase of nylon 6 respectively for all organoclay loading. Moreover, α-crystalline phase of nylon 6 was still appeared for all organoclay loading while the area of melting peak of γ-crystalline phase of nylon 6 decreased gradually with increasing organoclay loading. After heating, $M_2(HT)_2$ nanocomposite films were then cooled at the same rate, 10°C/min. DSC cooling profiles of $M_2(HT)_2$ nanocomposite films was shown in figure 5.9. The crystallization peak shifted to higher temperature when organoclay loading approached 1 wt%. However, the crystallization temperature of $M_2(HT)_2$ nanocomposite films occurred at the same temperature regardless the clay content.

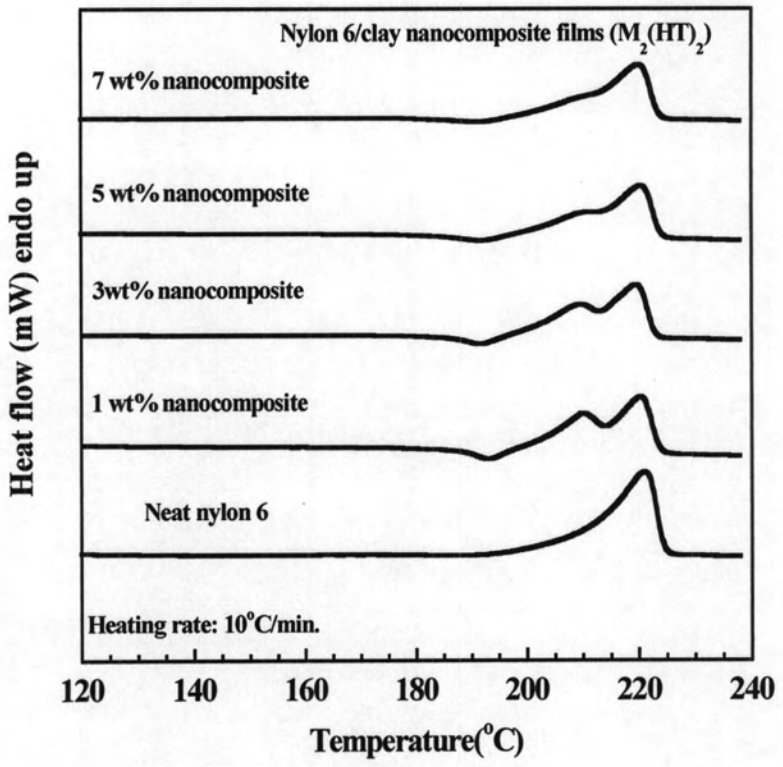

Figure 5.8: DSC heating profiles of nylon 6 and $M_2(HT)_2$ nanocomposite films at different organoclay loading.

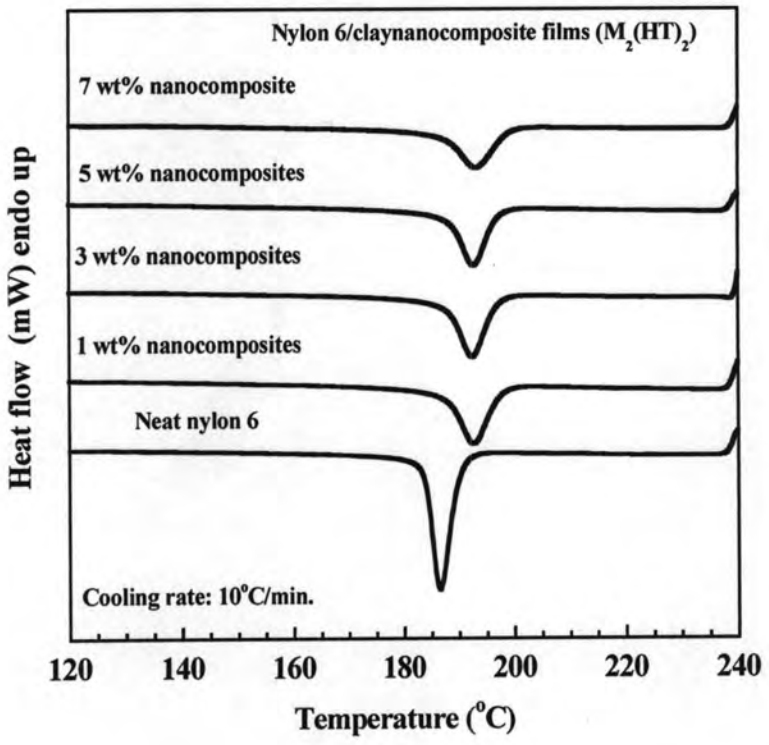

Figure 5.9: DSC cooling profiles of nylon 6 and $M_2(HT)_2$ nanocomposite films at different organoclay loading.

From above results, it should be noted that the addition of organoclay into nylon 6 matrix enhanced γ-crystalline phase of nylon 6 as shown in figure 5.6 and 5.8. Furthermore, the addition of layered silicates into nylon 6 matrix also enhanced the rate of crystallization, which could be observed from the increasing crystallization temperature with increasing organoclay loading into nylon 6 matrix as shown in figure 5.7 and 5.9. In other words, layered silicates served as an additional nucleating agent [7-8, 10]. However, the lower crystallization temperature could be observed at high organoclay loading because the diffusion of nylon 6 chains to be incorporated and formed as crystalline parts in the space between layered silicates was hindered at high organoclay loading which is consistent with Fornes and Paul's work [7].

5.3 Crystalline Structure of Nylon 6 in Nylon 6/Clay Nanocomposite Films

After observing an interlayer spacing of clay by XRD, the crystalline structure of nylon 6 was also investigated by x-ray diffraction technique from 2θ =18-28° whether there were any changes due to the presence of layered silicates.

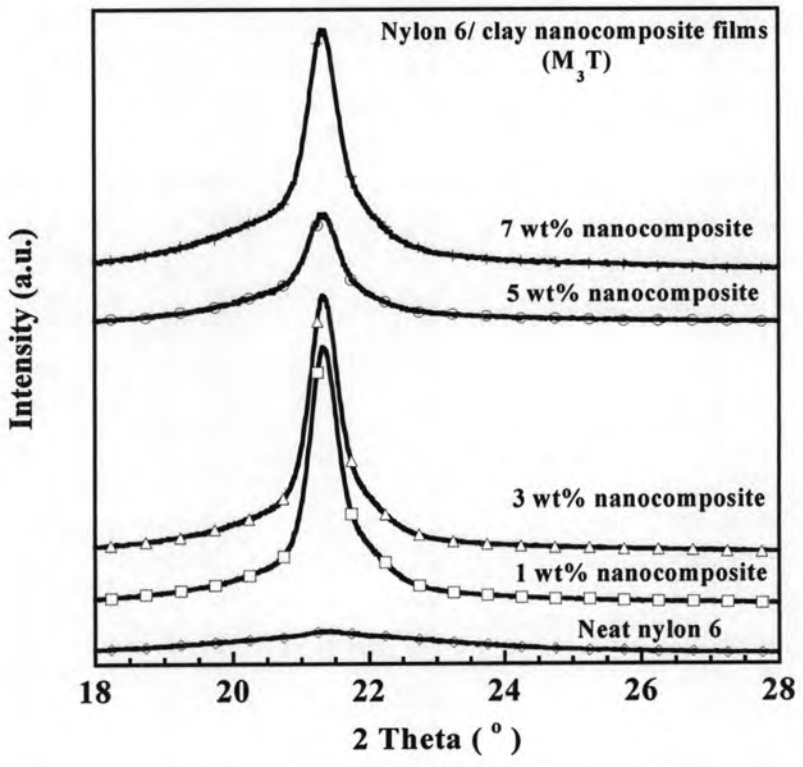

Figure 5.10: XRD patterns showing crystalline phase of nylon 6 and M_3T nanocomposite films at different organoclay loading.

Figure 5.10 presented XRD patterns of crystalline structure of neat nylon 6 and M_3T nanocomposite films with different organoclay loading. XRD peak at around 2θ =21.4° corresponding to γ-crystalline phase of nylon 6 was observed for neat nylon 6 and M_3T nanocomposite films. In addition, the area under diffraction peak (2θ=18-28°) was summarized in table G.21 (appendix G). It can be seen that the area under diffraction intensity of γ-crystalline phase of nylon 6 increased by 11.3 times when

organoclay loading was increased from 0 to 3 wt%. The increase in area under diffraction intensity indicated that the degree of crystallinity increased with increasing organoclay loading. This result indicated that the addition of organoclay enhanced the growth of crystalline part. In other words, layered silicates served as a nucleating agent. However, the area under diffraction peak of γ-crystalline phase of nylon 6 decreased when organoclay loading was further increased to 5 wt% and became increased again when organoclay loading was further added over 5 wt%.

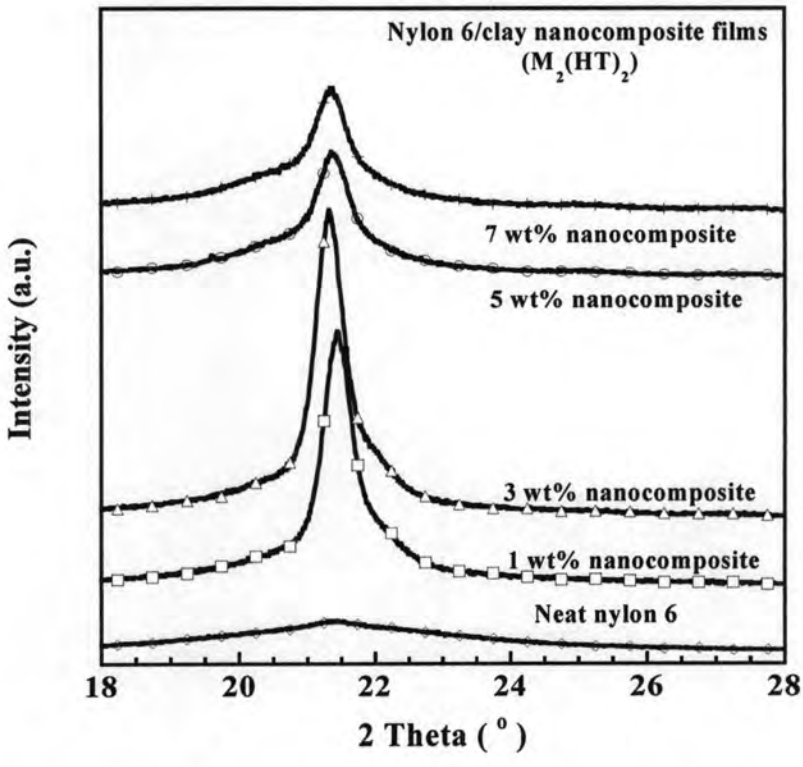

Figure 5.11: XRD patterns showing crystalline phase of nylon 6 and $M_2(HT)_2$ nanocomposite films at different organoclay loading.

From figure 5.11, the diffraction peak of γ-crystalline phase of $M_2(HT)_2$ nanocomposite films still appeared at the same 2θ value (2θ =21.4°) as M_3T nanocomposite films. However, the area under diffraction intensity of $M_2(HT)_2$ nanocomposite films was lower than that of M_3T nanocomposite films. In other words, the area under diffraction intensity of $M_2(HT)_2$ nanocomposite films increased by 9.6 times when organoclay loading was approached to 3 wt%. While the area

under diffraction intensity of γ-crystalline phase of nylon 6 in M_3T nanocomposite films increased by 11.3 times when organoclay loading was approached to 3 wt%. After organoclay loading approached to 5 wt%, the area under diffraction peak of γ-crystalline phase of nylon 6 decreased rapidly. This indicated that the degree of crystallinity decreased after organoclay was added over 3 wt%. This could be due to the limit of growth of crystallinity of nylon 6 between layered silicates when organoclay approached at high content which is consistent with Fornes and Paul's work [7]. After that the area under diffraction peak of $M_2(HT)_2$ nanocomposite films remained nearly the same level as the area under diffraction peak of $M_2(HT)_2$ nanocomposite films at 5 wt% of organoclay loading when organoclay loading was further added to 7 wt%.

Moreover, the degree crystallinity of the nanocomposite films was also calculated by the area under heating curves as summarized in table H.1 (appendix H). From figure 5.12, it can be seen that the degree of crystallinity increased with adding 1 wt% of organoclay but it decreased when organoclay was further added for both surfactants. The increase in degree of crystallinity is resulted from the addition of layered silicates and the capability of diffusion of nylon 6 chains to the growing crystallite as described above. This result is consistent with Jiang et al. [8].

However, the degree of crystallinity of nylon 6 matrix determined by the area under DSC heating curve was less precise than that of nylon 6 matrix calculated by the area under the diffraction intensity of XRD curve. In DSC technique, nanocomposite films were preheated to melt crystalline phase of nylon 6 during heating. Therefore nylon 6 chain can be rearranged and formed crystalline part. Consequently, the degree crystalline part may be decreased or increased after heating nanocomposite films. In XRD analysis, area under diffraction peak nylon 6 can identify the degree of crystallinity directly without the preheating of nanocomposite films. Therefore the degree of crystallinity determined by this technique was not accurate when compared with that by XRD technique. Therefore, the area under diffraction peak was chosen for later discussion.

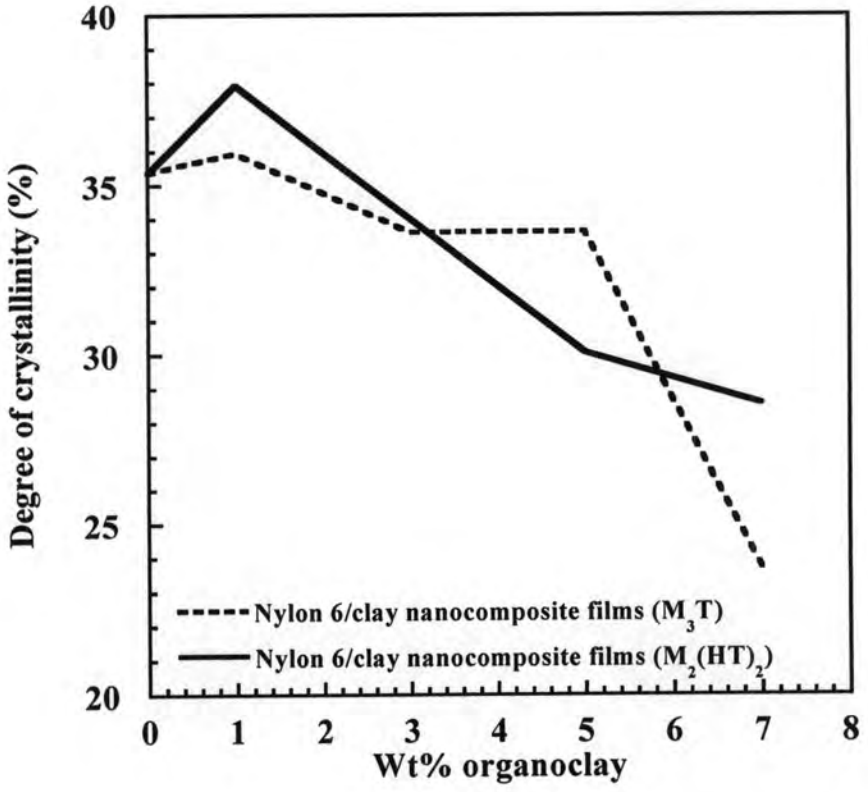

Figure 5.12: The degree of crystallinity of M_3T and $M_2(HT)_2$ nanocomposite films from DSC experiment.

5.4 Effect of Number of Long Alkyl Tail of Organoclay on Mechanical Properties of Nylon 6/Clay Nanocomposite Films

The mechanical properties of M_3T and $M_2(HT)_2$ nanocomposite films were shown in figure 5.13-5.18. The mechanical properties of M_3T and $M_2(HT)_2$ nanocomposite films in machinery direction were shown in figure 5.13-5.15. In this study, tensile test was used to determine the mechanical properties of nanocomposite films, which were tensile modulus, yield strength and elongation at break. Tensile modulus was used to indicate the stiffness of materials which was determined by the first linear slope of stress-strain curve. Yield strength of material was also used to identify maximum stress which materials began to deform. In addition, elongation at break was defined as strain at the rupture of the specimen. It was well known that

polymer/clay nanocomposites have attracted great interest due to the improvement of stiffness and other properties of materials. These improvements were resulted of inorganic material which serves as a reinforcement agent. Therefore the addition of inorganic materials into polymer matrix can help improving the stiffness of materials. However, interfacial interaction between polymer and layered silicates should be also considered because it strongly affected the improvement of mechanical properties. Inorganic contents at different organoclay loading of M_3T and $M_2(HT)_2$ nanocomposite films were summarized in table F.1 (appendix F). Besides inorganic materials, the crystalline part of polymer also enhances the stiffness of polymer. The stiffness of materials increases with increasing degree of crystallinity.

From figure 5.13-5.14, tensile modulus and yield strength of M_3T nanocomposite films increased with increasing inorganic content. In other words, tensile modulus and yield strength increased by 167 and 56 percent respectively when inorganic content was added to 3.88 wt% (7 wt% of organoclay loading). In similar trend, tensile modulus and yield strength of $M_2(HT)_2$ nanocomposite films increased by 30 and 29 percent respectively when inorganic content was added to 1.10 wt% (3 wt% of organoclay loading). After that they decreased slightly further when adding inorganic over 1.10 wt% (3 wt% of organoclay loading). The increase of tensile modulus and yield strength for both M_3T and $M_2(HT)_2$ nanocomposite films may be mainly caused by the addition of inorganic filler (organoclay) that acts as a reinforcement agent into nylon 6 matrix. However, the decrease of tensile modulus and yield strength of $M_2(HT)_2$ nanocomposite films may be resulted from the decrease of area under diffraction intensity after adding organoclay loading over 3 wt% (1.10 wt% of inorganic content) which was shown in figure 5.11. It meant that the degree of crystallinity decreased after inorganic content was added over 1.10 wt%. Consequently, this decrease of degree of crystallinity of nylon 6 matrix leaded to the lower stiffness of $M_2(HT)_2$ nanocomposite films. On the other hand, elongation at break of M_3T nanocomposite films as shown in figure 5.15 decreased by 51 percent when inorganic content increased to 3.88 wt% (7 wt% of organoclay loading). This indicated that the increasing inorganic content caused less ductility or more brittle because the addition of inorganic leaded to the higher stiffeness. The same trend of

elongation at break was also observed in $M_2(HT)_2$ nanocomposite at low inorganic content (0 to 1.83 wt% of inorganic content). After that elongation at break of $M_2(HT)_2$ nanocomposite films increased gradually with increasing inorganic further. This increase in elongation at break was resulted from the decrease in degree of crystallinity of nylon 6 as shown in figure 5.11.

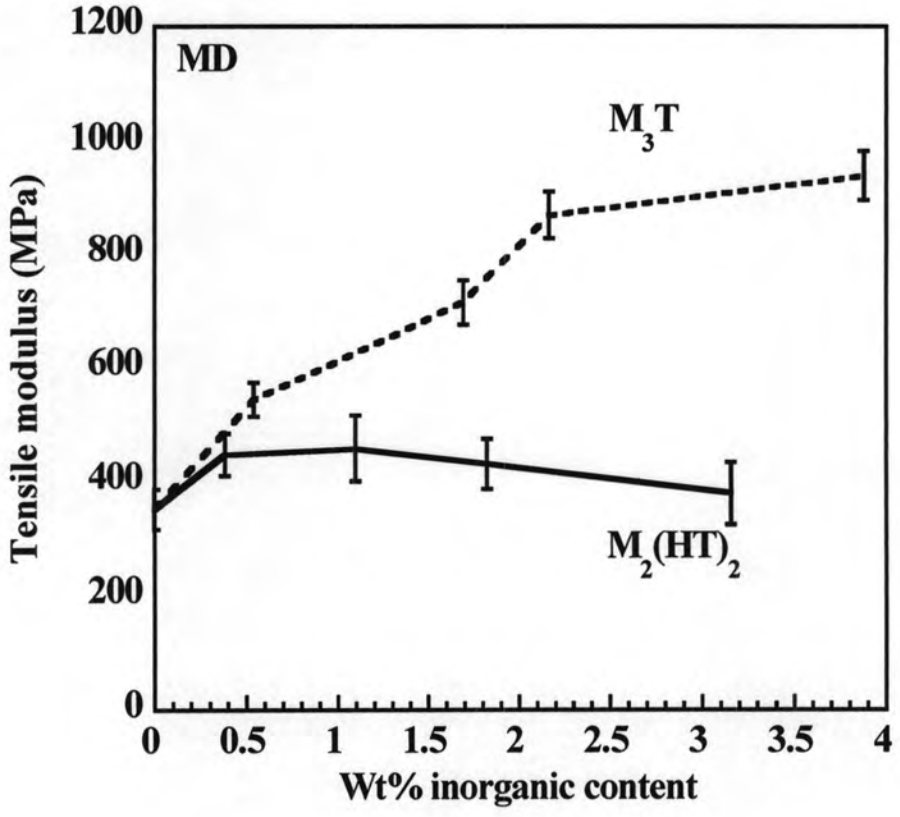

Figure 5.13: Tensile modulus of M_3T and $M_2(HT)_2$ nanocomposite films in machinery direction at different inorganic content.

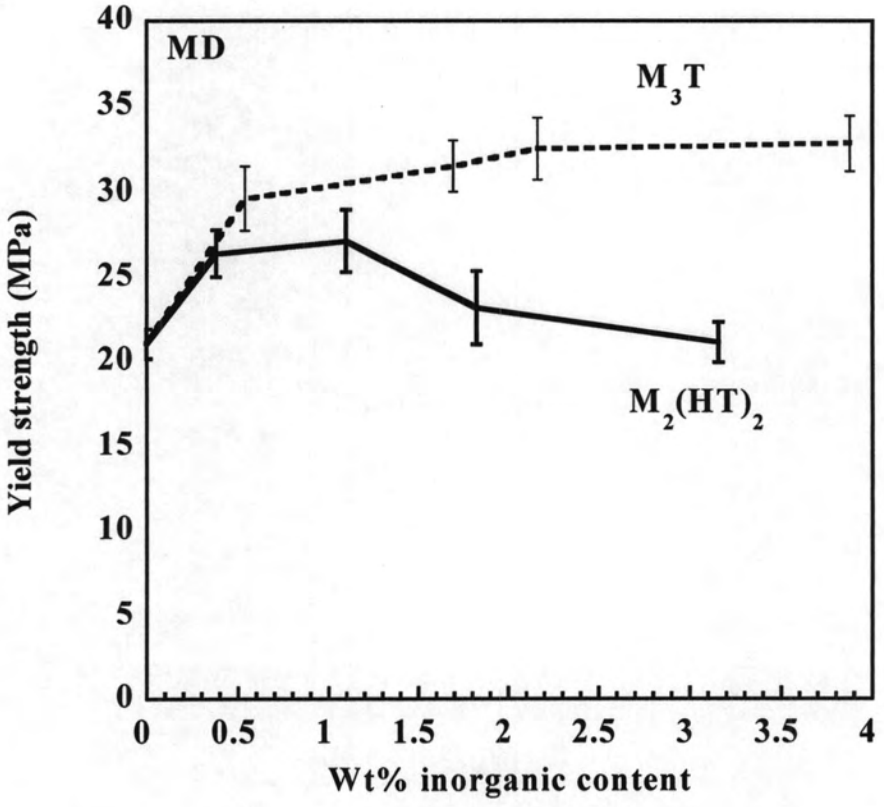

Figure 5.14: Yield strength of M_3T and $M_2(HT)_2$ nanocomposite films in machinery direction at different inorganic content.

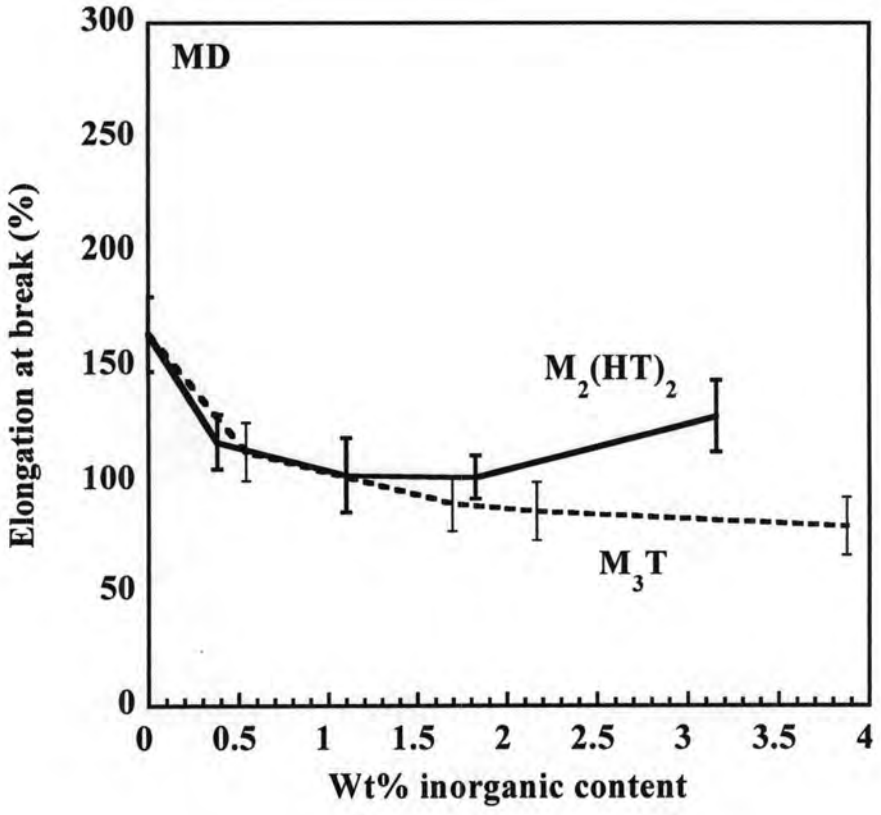

Figure 5.15: Elongation at break of M_3T and $M_2(HT)_2$ nanocomposite films in machinery direction at different inorganic content.

From figure 5.13-5.15, it indicated that M_3T nanocomposite films exhibited higher stiffness than $M_2(HT)_2$ nanocomposite films at any inorganic content. This could be due to the difference of access of nylon 6 chains to surface of layered silicates of nanocomposite films. It is well known that nylon 6 is high polarity and has a strong hydrogen bonding within and between polymer chains. Therefore, nylon 6 is high capability of access to polar surface of layered silicates. In addition, the structure of M_3T organoclay is smaller than that of $M_2(HT)_2$ organoclay. Therefore, the number of interactions between nylon 6 matrix and M_3T organoclay was higher than that of interactions between nylon 6 matrix and $M_2(HT)_2$ organoclay. This result is consistent with T.D Fornes [4]. These observations were confirmed by x-ray diffraction analysis that M_3T nanocomposite films exhibited higher interlayer spacing and distribution of layered silicates than $M_2(HT)_2$ nanocomposite films. Besides layered silicates that act as a reinforcement agent, the increase of degree of crystallinity of polymer also

enhanced the stiffness of materials. In XRD results at 2θ= 18-28° shown in figure 5.10-5.11, it was clear that the area under of diffraction intensity of M_3T nanocomposite films exhibited higher than that of $M_2(HT)_2$ nanocomposite films. In other words, the degree crystallinity of M_3T nanocomposite films was higher than that of $M_2(HT)_2$ nanocomposite films.

The same trends were also observed for mechanical properties of M_3T and $M_2(HT)_2$ nanocomposite films in transverse direction as shown in figure 5.16-5.18. Tensile modulus and yield strength of M_3T nanocomposite films increased with increasing inorganic content. In other words, tensile modulus and yield strength of M_3T nanocomposite films increased rapidly by 79 and 41 percent respectively when inorganic content was added to 2.16 wt% (5 wt% of organoclay loading). After that they were nearly constant at higher inorganic content further. This increase in tensile modulus and yield strength was caused by the addition of inorganic which serves as a reinforcement agent. However, elongation at break decreased by 28 percent when inorganic content was added to 3.88 wt% (7 wt% of organoclay loading). This indicated that the increasing inorganic content leaded to a higher stiffness material and caused more brittle as discussed above. For $M_2(HT)_2$ nanocomposite films in transverse direction, elongation at break and yield strength exhibited the same trend as those in machinery direction as shown in figure 5.14 and 5.15 while tensile modulus was nearly constant.

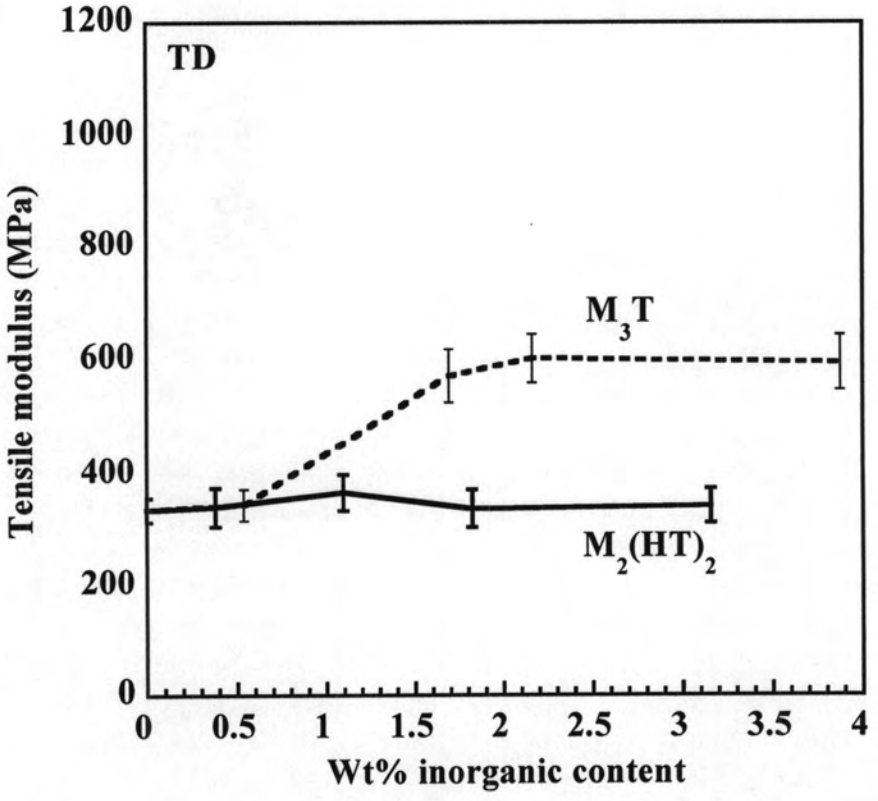

Figure 5.16: Tensile modulus of M_3T and $M_2(HT)_2$ nanocomposite films in transverse direction at different inorganic content.

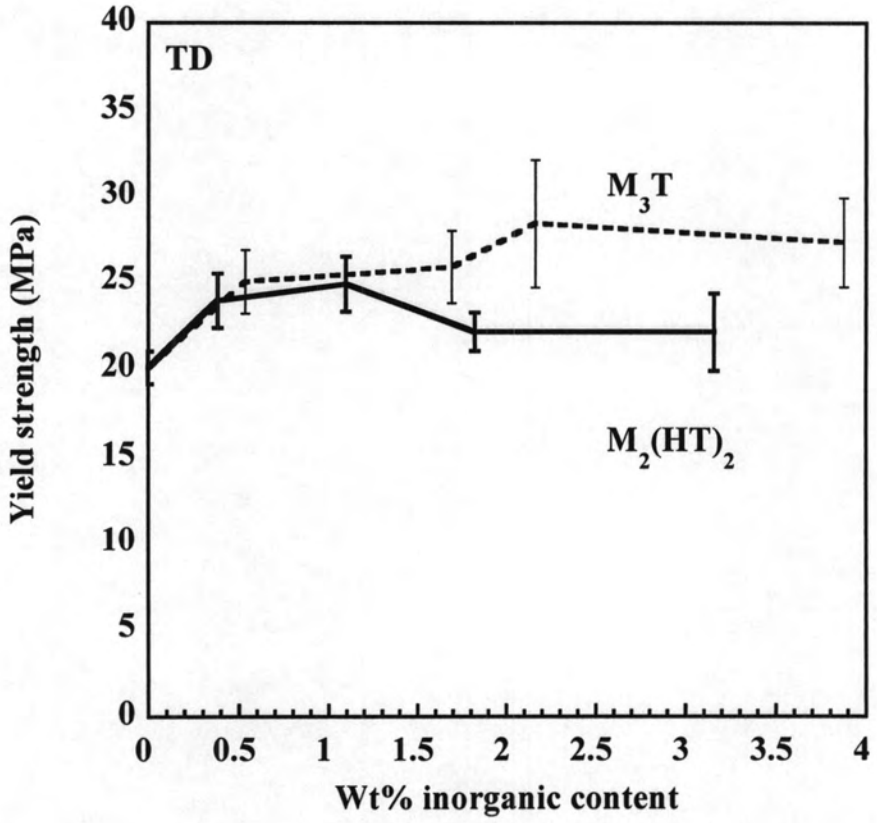

Figure 5.17: Yield strength of M_3T and $M_2(HT)_2$ nanocomposite films in transverse direction at different inorganic content.

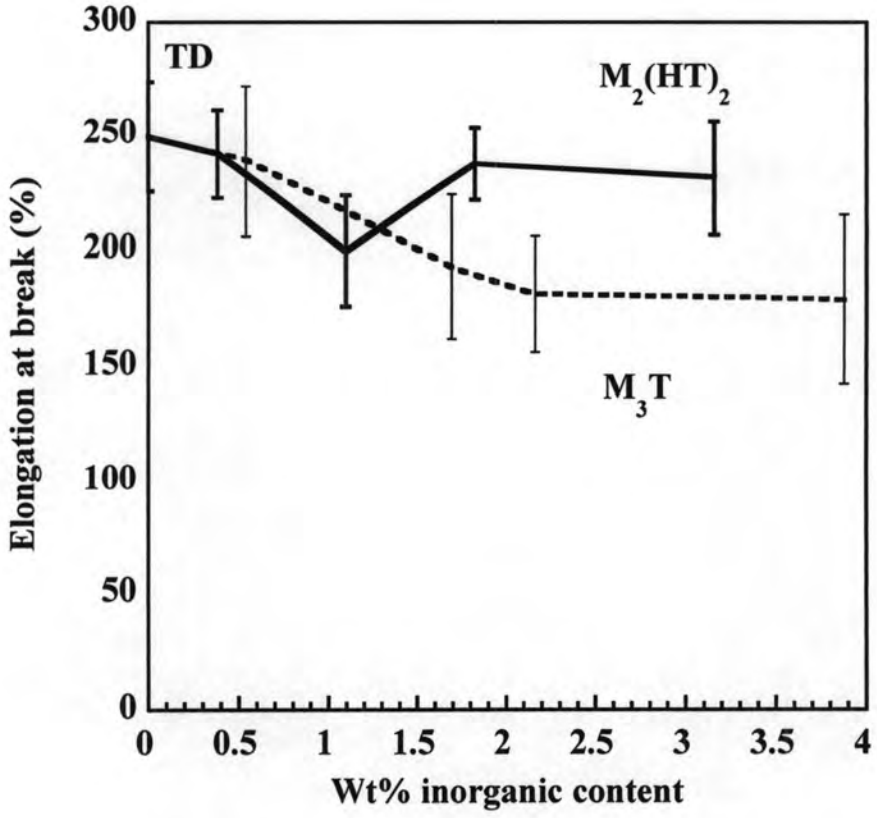

Figure 5.18: Elongation at break of M_3T and $M_2(HT)_2$ nanocomposite films in transverse direction at different inorganic content.

The orientation of layered silicates affected strongly the mechanical properties of nanocomposite films. In addition, the orientation of polymer chains also affected the mechanical properties. In this process, nanocomposite films were formed by using twin screw extruder attached to blown film die. Therefore, the degree of orientaion of layered silicates and polymer chains should be considered. From figure 5.13 and 5.16, tensile modulus of nylon 6 film was nearly equal in both directions. However, adding 3.88 wt% inorganic content into nylon 6 matrix, tensile modulus increased rapidly by 167 percent in machinery direction but only 77 wt% in transverse direction. The layered silicates would arrange themselves in the direction that was in the same plane as machinery direction plane of film but not totally in the same plane as transverse direction plane of film. Therefore, layered silicates would reinforce polymer film in machinery direction more than in transverse direction.

5.5 Barrier Performance of Nylon 6/Clay Nanocomposite Films

The oxygen permeability of M_3T and $M_2(HT)_2$ nanocomposite films at different inorganic content was shown in figure 5.19. From this figure, the oxygen permeability of M_3T nanocomposite films decreased continuously by 27 percent at 2.16 wt% of inorganic content (5 wt% of organoclay loading) when compared with neat nylon 6 film. In other words, the oxygen permeation resistance of M_3T nanocomposite films was better than that of neat nylon 6 films. The same trends were also observed in $M_2(HT)_2$ nanocomposite films at low inorganic content (0-0.38 wt%). Oxygen permeability decreased when inorganic content was added to 0.38 wt% (1 wt% of organoclay loading). However, oxygen permeability increased gradually with increasing inorganic content later. The decrease of oxygen permeability was resulted from the addition of layered silicates into nanocomposite films, which created the tortuous pathways of oxygen. In addition, XRD and TEM results as shown in figure 5.2-5.5 confirmed that M_3T nanocomposite films exhibited broader distribution of layered silicates than $M_2(HT)_2$ nanocomposite films. This indicated that the dispersion of layered silicates in M_3T nanocomposite films were better than those in $M_2(HT)_2$ nanocomposite films. This better dispersion leaded to much increase in tortuous pathway that oxygen passed through nanocomposite films. Consequently, oxygen permeation resistance of M_3T nanocomposite films was higher than that of $M_2(HT)_2$ nanocomposite films. Not only layered silicates enhanced oxygen permeation resistance but the increasing in crystalline phase of nylon 6 also improved oxygen barrier resistance because the crystalline phase of nylon 6 matrix could hinder the permeation of oxygen through nanocomposite films. Moreover, the interlayer spacing of γ-crystalline phase of nylon 6 which appeared in neat nylon 6 and nanocomposite films in XRD and DSC results was lower than that of α-crystalline phase of nylon 6 (see in table 2.3). This decreasing interlayer spacing of γ-crystalline phase of nylon 6 could reduce the free volume of nylon 6. Consequently, oxygen permeation resistance further increased. However, the increase oxygen permeation of $M_2(HT)_2$ nanocomposite films after adding over 0.38 wt% of inorganic content (1 wt% organoclay loading) caused by the decrease of degree of crystallinity as shown in

figure 5.11 and the narrow distribution of layered silicates in $M_2(HT)_2$ nanocomposite films as shown in figure 5.4. This result is consistent with Jiang et al. [8].

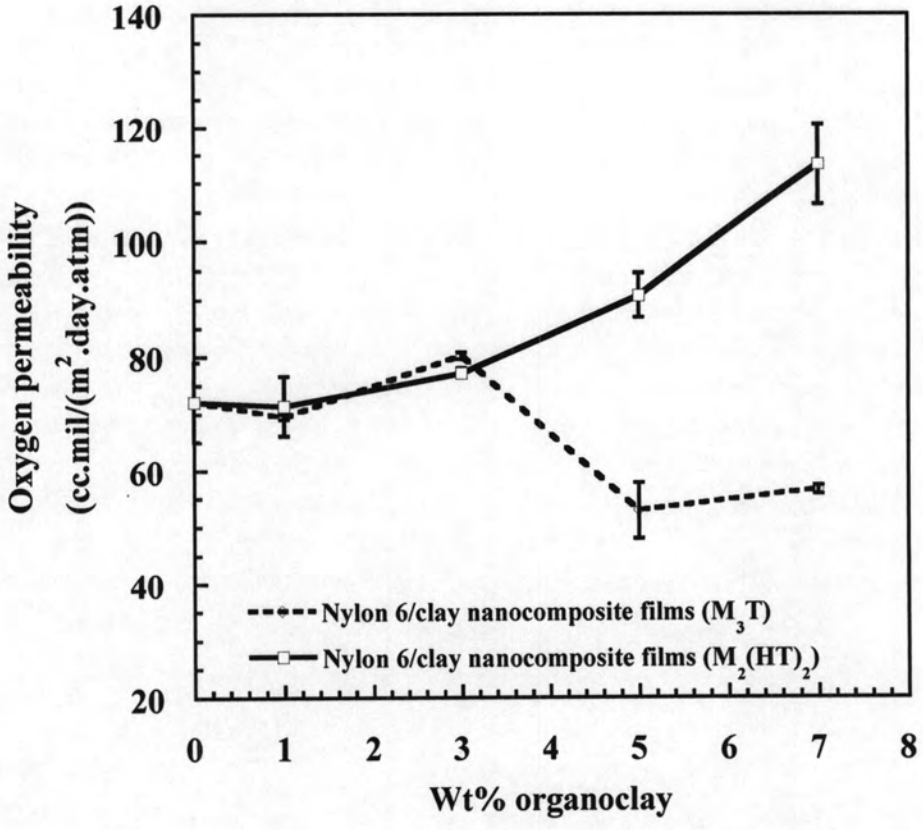

Figure 5.19: Oxygen permeability of M_3T and $M_2(HT)_2$ nanocomposite films at different organoclay loading.